Optics Communications 281 (2008) 4261–4267

Contents lists available at ScienceDirect

Optics Communications

journal homepage: www.elsevier.com/locate/optcom

Modeling high density microholographic data storage: Using linear, quadratic, thresholding and hard clipping material characteristics

Balázs Gombkötő [a,*], Zsolt Nagy [b], Pál Koppa [a], Emőke Lőrincz [a]

[a] Department of Atomic Physics, Budapest University of Technology and Economics, Budafoki út 8, H-1111 Budapest, Hungary
[b] Holografika Kft. Pf. 100, H-1704 Budapest, Hungary

ARTICLE INFO

Article history:
Received 19 November 2007
Received in revised form 21 March 2008
Accepted 22 April 2008

Keywords:
Holographic and volume memories
Volume holographic gratings
Inhomogeneous optical media

ABSTRACT

Crosstalk related raw signal-to-noise ratio (SNR) and bit error rate (BER) of high density bitwise microholographic data storage is investigated by numerical modeling. Scattering and diffraction of light is calculated in non-paraxial scalar approximation. A multiple thin slice implementation of the perturbative volume integral equation is used, which can be easily parallelized. The effect of bit and track spacing, and the different local characteristics of the holographic recording material on the SNR, BER and diffraction efficiency are investigated. The results show that these lateral spacing parameters have much more effect on crosstalk noise than the number of layers. Using two-photon, thresholding or hard clipping materials generates less crosstalk noise at the same data density than a linear material, and the dynamic range of these materials can be used more effectively resulting in higher single microhologram diffraction efficiencies.

1. Introduction

Microholographic data storage [1] is one of the best candidates for future high capacity optical memories. DVD based bitwise data storage systems are able to have up to four 2D data layers, and eight layer systems exist in laboratory environment offering 200 GByte user capacity per disk. Further growth of the number of layers is strongly limited by inter-layer crosstalk, besides, beam filtering and disk manufacturing is also a critical issue. Using *reflective* microholographic volume gratings instead of pits has a benefit from the 3D shift selectivity of holographic readout, i.e. neighboring bits/holograms are read out not only partially but phase mismatched as well, and therefore their contribution to the detector signal is weaker. Using a so called confocal filter further improves the suppression of crosstalk. The filter is placed to the optical image of the addressed bit, where the backscattered/reconstructed signal beam is being focused. Due to similar data encoding and bitwise storage, the required opto-mechanical system is highly compatible with existing DVD technology. The microholograms are generated by the interference of two counter propagating focused beams in an appropriate recording material. Being a critical issue, such holographic materials are intensely researched worldwide [2–7] to fulfill the requirements of present and future holographic data storage systems. Experimental results on the method also exist in the literature [8–10].

In this paper, we present a numerical model of microholographic data storage, which is able to simulate the crosstalk of more than 20 data layers on a single desktop computer. The method can be adapted to parallel computation effectively and only 2D arrays have to be stored in the computer memory. Raw signal-to-noise ratio (SNR) and bit error rate (BER) values are obtained from energy histograms produced by the model. Several parameter configurations were tested regarding bit spacing, track spacing, layer spacing distances, and material characteristics. The results show good agreement with our previous modeling tool [11]. The relation of inter-layer crosstalk, material dynamic range and single bit diffraction efficiency is also discussed.

2. Optical modeling

The 3D model of the optical setup can be seen in Fig. 1. The counter propagating focused object and reference beams expose the microholographic gratings one-by-one inside the recording layer, when an ON bit is to be stored. During the readout the focused readout beam scans the middle data layer in the exact locations of the bits by shifting the layer in the lateral directions. The summed intensity of the backscattered light after the confocal filter is registered, and the collected data set is compared to the set of bits written in order to build an energy histogram of the ON and OFF bits. The histogram is further analyzed for deriving BER and SNR values.

The simulation consists of three parts: the first part generates the focused writing and reading beams using a wave-optical lens

* Corresponding author. Tel.: +36 1463 1457; fax: +36 1463 4180.
E-mail address: gombkoto@eik.bme.hu (B. Gombkötő).

0030-4018/$ - see front matter © 2008 Elsevier B.V. All rights reserved.
doi:10.1016/j.optcom.2008.04.057

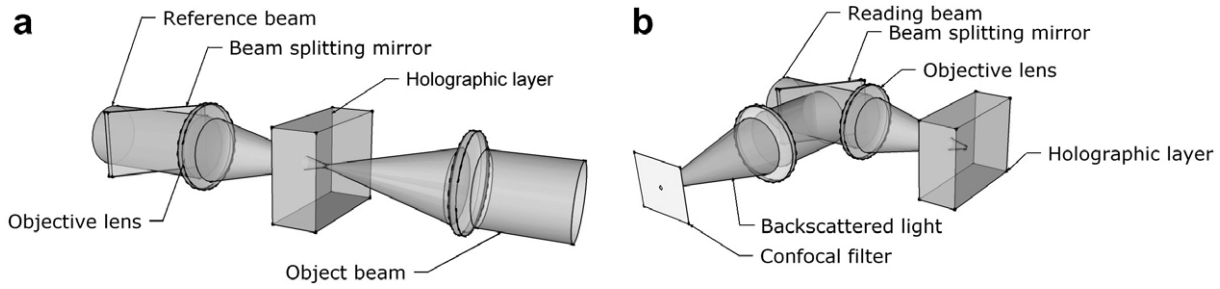

Fig. 1. The graphics 3D model of the optical setup: (a) the writing and (b) the reading process (transmitted light is not shown).

model and scalar diffraction. The second part generates the interference pattern of the writing beams using scalar wave propagation and the sum exposure due to the ON bits inside the whole recording layer, and diffracts the reading beam on this complex grating. The third part generates the detector signal from the backscattered/reconstructed beam using spatial filtering. Index matching is used, i.e. the mean refractive index is 1.5 everywhere in the model. Due to this matching beam aberrations at layer boundaries are omitted, which results in a focusing being independent from the axial position of the bits.

2.1. Beam focusing

The beams used for writing and reading are produced using the scalar version of the method in Refs. [12–14]. The aperture (or entrance pupil) of the focusing lens is illuminated with a uniform plane wave. The lens itself is modeled as a phase transformation element: the phase of an ideal spherical wave is added to the phase of the incident plane wave. The light is propagated from the lens (exit pupil) to a plane near the focus point using the modification of the well-known Fourier-transform based plane wave spectrum propagator method, or sometimes referred as the convolution method [15]. The sampling problems due to the large beam diameter by the lens and strong convergence of the beam (NA = 0.6) is avoided by introducing an artificial separation of the wave phase into two terms [12]. This results in an additional Fourier-transformation in the method, and due to that the sampling distances, i.e. the scales of the described fields can be different in the input and output planes of the calculation. Based on the similar property of the Fresnel-transformation and because this method is *not* paraxially limited, it is sometimes referred as the extended Fresnel-method. The detailed derivation and implementation can be found in the given references.

2.2. Inside the recording layer

The second part models the propagation of the writing and reading beams, the scattering of the reading beam on the grating, the exposure process, and the propagation of the scattered beam, all inside the recording layer. Due to the spatial overlapping of the individual microholograms the exposure per bit is small, and considering the otherwise also weak grating (index modulation of 10^{-2} and below) of a saturated exposure in a typical photopolymer material, the diffraction efficiency will be low (10^{-4} and below). Hence, the first-order approximation of the Born-series expansion of the diffracted field is satisfactory, which physically means single scattering only. In this case the total electric field is the sum of the incident reading beam and the first-order diffracted field [16]:

$$E(\mathbf{r}) + E_0(\mathbf{r}) + E_1(\mathbf{r}) = E_0(\mathbf{r}) + \frac{k_0^2}{4\pi}\iiint_V G(|\mathbf{r}-\mathbf{r}'|)\cdot P_{\text{pert}}(\mathbf{r}'))\mathrm{d}V', \qquad (1)$$

where E_0 is the incident reading beam, G is an integral kernel (or Green function) related to wave propagation/diffraction, k_0 is the length of the wave vector in vacuum, P_{pert} is the perturbative polarization which is proportional to the dipole polarization density due to the readout, and acts as the source distribution of the scattered field. The integration domain V is the finite effective volume of the whole grating or a volume that includes it. In a holographic case the source P_{pert} can be defined as follows [17]:

$$P_{\text{pert}}(\mathbf{r}') = \omega^2\mu_0\delta\varepsilon(\mathbf{r}')E_0(\mathbf{r}'), \qquad (2)$$

where $\delta\varepsilon$ is the (isotropic) permittivity modulation, ω is the angular frequency of the light, and μ_0 is the magnetic permeability in vacuum. The physical meaning of this formula is holographic reconstruction: while the incident beam E_0 locally reads out the permittivity modulation, and $\delta\varepsilon$ is related to the (incoherent) sum of gratings described by $|E_{\text{ref}} + E_{\text{sig}}|^2$ like terms of holographic exposures, some terms in the expansion of P_{pert} will be related to three-wave products $E_{\text{sig}}E_{\text{ref}}^*E_0$ (* here stands for complex conjugate). If the readout beam is the same as the reference beam of an ON bit/microhologram, the object beam of that bit will be reproduced. Thus, Eq. (2) can be regarded as a form of the basic equation of holography.

The regular way to evaluate the above volume integral is based on the fact that it is a convolution integral, therefore it can be implemented using fast Fourier-transformations (FFT) [18]. The 3D FFTs of 3D arrays can be done very fast, if all necessary arrays fit in the computer memory. Due to the large number of layers and bits per layer, i.e. the large volume of the whole grating, this implementation cannot be used in our case. But single scattering also means that the total first-order diffracted field is the coherent sum of fields emerging from different sub-volumes of the whole volume, or with other words the sub-volumes contribute to the total scattered field $E_1(\mathbf{r})$ independently. From the viewpoint of discretization these sub-volumes can be thin slices as well: lateral planes with the numerical sampling distance Δz as their third dimension. This kind of sub-division will reduce computational requirements to 2D arrays. The principle of the calculation is depicted in Fig. 2, and is formulated as follows [19]:

$$E_1(z_0) = \frac{k_0}{2}\int_{z1}^{z2} \mathrm{IFT}[H(f_x,f_y;\ z_0 - z)\cdot \mathrm{FT}[P_{\text{pert}}](f_x,f_y;\ z)]\mathrm{d}z \qquad (3)$$

where FT[··] and IFT[··] stand for the forward and inverse 2D Fourier-transformation along the x and y coordinates, f_x and f_y are spatial frequencies regarding to these coordinates, $H = \mathrm{FT}[G]$ is a transfer function describing wave propagation, and the integration on the z axis (optical axis) goes through the whole thickness of the holographic layer. Simply dividing the [$z1$, $z2$] interval, this algorithm can be run parallel on more computers. While only far field diffraction reaching the detector is interesting, the usual plane-wave spectrum propagator can be used as H[15]. As a summary, all the writing, reading and scattered beams are propagated by a $H(f_x, f_y, z_0–z)$ transfer function inside the recording layer, and scattering/holographic diffraction is described by Eq. (2) locally

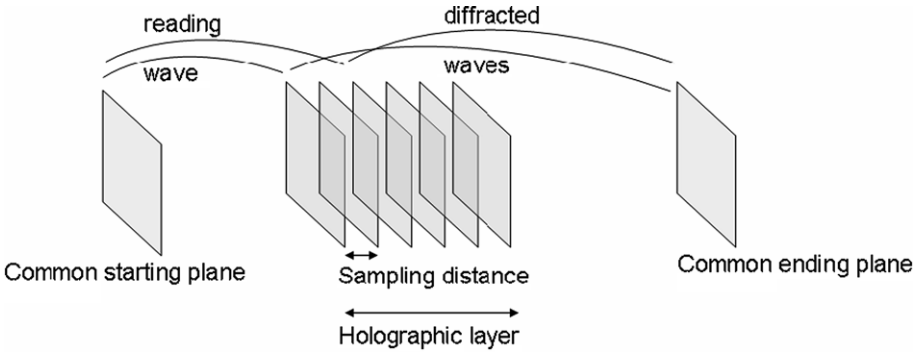

Fig. 2. The multiple thin slice implementation of the volume integral equation in first-order Born approximation. In this approximation sub-volumes of the holographic layer are independent.

and Eq. (3) globally. Note, that page based shift multiplexed holographic data storage was modeled previously using a similarly built model and implementation with success [20].

The $\delta\varepsilon$ exposure in all lateral sections of the recording layer was calculated as the sum effect of all the $N_xN_yN_z$ bits written. The N_x and N_y number of bits to write and the N_{rx} and N_{ry} number of bits to read was determined from the number of bit-layers (N_z), bit spacings in the three dimensions, and the NA of the beams so, that the crosstalk due to spatial overlaps during the writing and the reading are both fully developed. (Reading more bits from the middle layer, or writing less bits in any dimension would not model crosstalk correctly, since the reading beam would pass through "empty" parts of the material). Due to the separation of the exposed volume along the optical axis, this implementation of the volume integral does not make it possible to follow the one-by-one exposure of bits temporally. This means that there are no "previously written" bits, which could affect the exposing beams of the "currently recording" bit with their gratings or the low spatial frequency index change. According to the assumption that single bit gratings and the overall grating are both weak, this necessarily neglected effect can be estimated to be small.

2.3. Processing the scattered field

According to Fig. 2 the total E_1 field backscattered from all the ON bits (the actual micrograting) – with a main contribution from the addressed bit – is collected in a lateral plane somewhere outside the recording layer. In our reflective case this plane is on the same side of the layer, where the reading field is entering it. In the third part of the optical modeling this field is further processed. First, it is propagated back to the middle of the recording layer, again, using the standard convolution method (H as a transfer function), which means that this propagation is in homogeneous medium. This lateral plane in the middle of the layer is the plane which would be imaged in an actual microholographic system. This also means that the actual confocal filter has an image here, so confocal filtering can be performed without any additional diffraction modeling, provided that the aperture stops of the lenses performing the actual imaging has a negligible effect. The radius of the confocal filter is set to 1.2× the radius of the first null of the Airy-pattern. This radius can be calculated from the wavelength and the NA of the system as 0.61λ/NA. The filtered intensity distribution is then summed up to produce a detector signal (ideal linear detector characteristics is assumed). The $N_{rx}N_{ry}$ detector signals are compared to the original bits written in order to build two histograms (discreet probability density function, PDF) of the ON and OFF bits separately. From the statistical analysis of the histogram data the raw SNR and BER of the modeled system can be estimated. For example the SNR is formulated as follows [21]:

$$\mathrm{SNR} = \frac{|\mu_{\mathrm{ON}} - \mu_{\mathrm{OFF}}|}{\sqrt{\sigma_{\mathrm{ON}}^2 + \sigma_{\mathrm{OFF}}^2}}, \tag{4}$$

where μ and σ are the mean and variance of the corresponding intensity distributions. To calculate the overlapping integral needed to obtain the BER[21], the histogram curves were extrapolated. Since the curves have approximately Gaussian tails, the logarithm of these is quadratic, and second order polynoms can be fitted on them.

3. Results with linear material characteristics

Using the above described scalar wave-optical model of microholographic data storage we have performed simulations with the following parameters. The wavelength was 405 nm, the numerical aperture of the system and the beams was 0.6, and the sampling distances were 200 nm by 200 nm by 50 nm along the x, y and z coordinates, respectively. With these parameters the confocal filter has a radius of $1.2 \times r_{\mathrm{Airy}} = 1.2 \times 411.75$ nm = 494.1 nm. The number of data layers varied from 7 to 23. More layers (and consequently more bits per layer) could also fit in the 8 GByte memory of our computer, but the runtimes would have exceeded one month with a dual-core CPU. As an example, the number of stored bits per layer was 127×85 at 23 layers, and the middle 21×21 bits were read out from the middle layer. The largest matrices used in our modeling were 3072 by 3072 sized. When talking about linear material characteristics we consider single-photon processes, which mean that the relative permittivity changes linearly with intensity: $\delta\varepsilon\delta\tau/I$ ($\delta\tau$ stands for a time interval). The saturation properties of materials are not discussed in this paper: it is supposed that a proper exposure schedule is used achieving equal grating strength for all microgratings. Fig. 3 shows an example to the total exposure in a lateral xy plane in the case of seven data layers, bit spacings of 400 nm by 600 nm and layer spacing of 4 μm. The change of the relative permittivity versus numerical co-ordinates is shown right in the middle of the whole recording material, and also the middle (fourth) data layer. Exposure from the other six data layers is clearly visible as a diffuse background.

Using a material with linear characteristics, an exposed microhologram will cause equal overall exposure in all data layers (see also later), thus the dynamic range of the material, i.e. the saturated exposure has to be divided among the layers equally. This results in small single microhologram diffraction efficiency. If exposure scheduling is used, the total exposure will look like the one in Fig. 3, thus the modeled detector signal histrograms and the SNR and BER values derived from them can be regarded as results being valid for saturating single-photon materials, such as photopolymers.

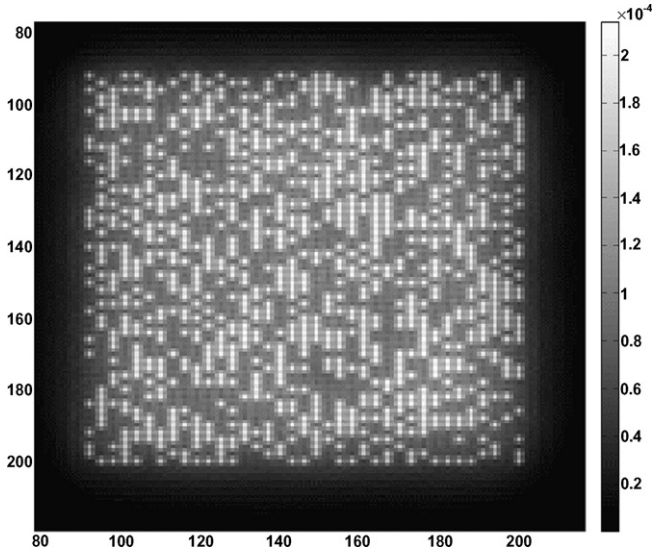

Fig. 3. Relative permittivity change in the middle of the recording layer in the case of seven data layers. Exposure from neighboring data layers causes a diffuse background (the co-ordinates are numerical sampling points, 55 × 37 bits were exposed per layer).

Fig. 4 shows a plot of the 50 step energy histograms of the ON (1) and OFF (0) bits in the case of 23 data layers. While the curve of the OFF bits has a roughly Gaussian shape, the curve of the ON bits show several local peaks, which is in agreement with the general physical picture: the signal of the OFF bits has a noise statistics, while the signal of the ON bits is strongly influenced by the interference with first-neighbor ON bits, which are responsible for the local peaks.

Table 1. shows the change of the raw SNR and BER versus different bit spacings in the case of seven data layers. It is seen, that these parameters have strong influence on crosstalk when a linear material is used. Note, that the estimated BER values are based on

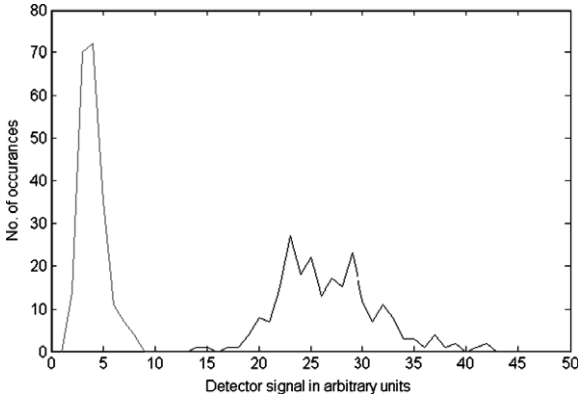

Fig. 4. The histogram of the detector signals for the total of 441 ON and OFF bits in the case of 23 data layers.

Table 1
Crosstalk related SNR and BER versus different bit/track spacings in case of a linear material characteristics

Bit spacings in microns	Layer spacing in microns	SNR	BER
0.8 × 0.8	4	10.6	3e-19
0.6 × 0.6	4	7	2.9e-6
0.4 × 0.6	4	4.3	4.7e-4

Table 2
The SNR of crosstalk related noise versus the number of data layers in case of a linear material characteristics

Number of layers	SNR
7	4.3
11	4.6
15	4.8
19	4.43
23	4.61

extrapolations, therefore strongly depend on the resolution of the histograms they are based on.

Table 2 shows the change of the raw SNR of *crosstalk related* noise versus the number of layers, when the spacings are the same as in the last line of Table 1. The SNR is about 4.5, but shows significant fluctuations due to the small statistics (about 400 bits per histogram).

4. Non-linear recording materials

The typical candidates of present and future holographic data storage systems are photopolymer materials. Generally, both polymerization and monomer diffusion has to be modeled together with exposure schemes, but in a large scale system model simple and fast running methods are needed. The net result of the two effects in a photopolymer is some degree of saturation of the material when exposed to light. In our microholographic system the holograms are reflective along the optical axis, so the main variation of the gratings is along that axis. Due to the previously described implementation of Eq. (1) 3D diffusion cannot be modeled, while successive z = const. planes are treated independently. However, local material characteristics can be modeled, such as non-linearities and saturation. In our simulations three other material behaviors were also embedded in the optical model beside the above discussed linear one.

The application of two-photon materials (where the change of the relative permittivity is quadratic in intensity $\delta\varepsilon\delta\tau/I^2$) is straightforward in non-holographic high density optical data storage [22]. Some photopolymers can show two-photon characteristics [23], and other types of materials can also have this kind of behavior [24]. These can also be used to record holographic gratings, but they will cause non-sinusoidal grating profile due to the non-linearity. Having a linear material characteristics the longitudinal grating profile (on the optical axis) copies the longitudinal intensity profile, which is depicted in Fig. 5c. As one can see, the profile has "sidelobes" partly shown in the figure. These sidelobes imagined in 3D have smaller peak intensities, but affect larger volumes, which results in a net effect of equal exposure in all data layers. Compared to Fig. 5c the quadratic intensity dependence shown in Fig. 5b results in a longitudinal grating profile (again on the optical axis) shown in Fig. 5a. According to this figure the exposed microhologram is more compact, has negligible relative permittivity change in other data layers compared to the change in the addressed layer, and as our modeling results show, the diffracted beam has a focus spot in the plane of the confocal filter having a similar size, as with the linear material. Besides the central spot some weak, higher order diffraction is also present as rings, but they are completely our of the confocal filter's range. Due to the quadratic intensity dependence a significant total change (after all bits are exposed) in the relative permittivity will only be made in the addressed layer, where the intensity is high. Having negligible change in the other layers their dynamic range will not be reduced. Compared to the linear case this will allow an increased single bit diffraction efficiency due to the more effective use of the dynamic range of the material.

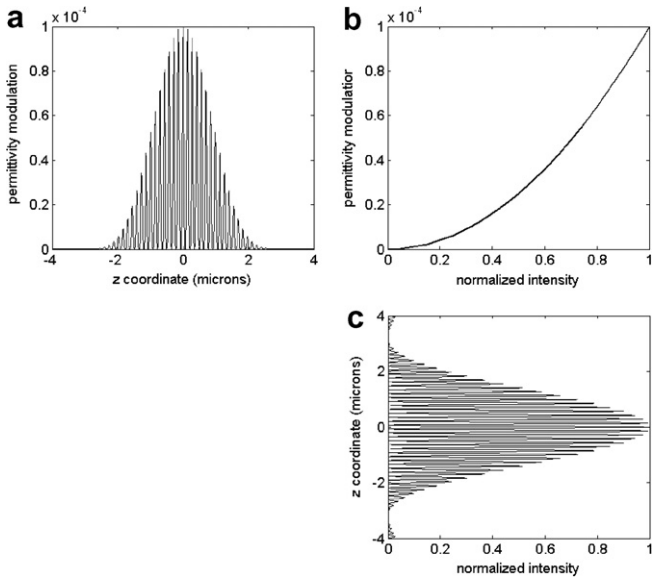

Fig. 5. a) The longitudinal exposure profile of a microhologram having quadratic material characteristics and using diffracting beams. b) The quadratic characteristics. c) The longitudinal intensity distribution normalized. Longitudinal "sidelobes" of the relative permittivity change are negligible.

A more detailed explanation of this main difference between linear and non-linear material characteristics is the following. When recording a microhologram into a specific layer all other layers are exposed by the same total flux, since both the signal and reference beams traverse the entire disk. Thus for conical beams focused on the addressed layer from a non-apodized aperture exposure intensity will decrease in inverse proportion with the beam cross section:

$$I_j \propto \left[\frac{1}{(j - j_{\text{addr}}) \cdot \mathrm{d}_{\text{layer}}}\right]^2 \quad \text{for all } j \neq j_{\text{addr}}, \tag{5}$$

where d_{layer} is the layer spacing, j_{addr} and j are the index numbers of the addressed layer and the other layers. When serially exposing all other holograms in the addressed layer a small area in another layer under investigation will receive further exposure as many times as the writing and reading conical beams overlap the area:

$$t_j \propto WR \cdot [(j - j_{\text{addr}}) \cdot d_{\text{layer}}]^2, \tag{6}$$

where t_j is the *overall* exposure time at any point of a non-addressed layer and WR is the "white rate" of the encoded data (the probability of ON bits). In linear recording materials the average permittivity change is proportional to the total exposure flux density (intensity × exposure time):

$$\Delta\varepsilon_j \propto I_j \cdot t_j = \text{const.} \tag{7}$$

Thus the recorded average permittivity change is the *same* in all layers independently from their distance from the addressed layer. In consequence if one wishes to have equal diffraction efficiency for all layers, a writing strategy has to be used that divides the material dynamic range equally among *all* the layers (note that this estimation is also valid for Gaussian or more complex focused beams if the Rayleigh range is smaller than the layer spacing, which is the case for our geometry).

However, for quadratic materials the average permittivity change is proportional to the square of the intensity × exposure time, and that will be:

$$\Delta\varepsilon_j \propto I_j^2 \cdot t_j \propto \left[\frac{1}{(j - j_{\text{addr}}) \cdot d_{\text{layer}}}\right]^2. \tag{8}$$

In this case the recorded average permittivity change is reduced as squared inverse of the distance of a layer from the addressed layer, so (relative to the addressed layer) there will be no exposure for distant layers and very little use of dynamic range for the neighboring layers. For thresholding type materials (discussed below) the writing intensity can be selected such that it only exceeds the sensitivity threshold for the addressed layers. That avoids the use of dynamic range in any other layers. From this we can conclude that the dynamic range requirement scales with the number of layers in the linear case, and stays constant in other cases.

Two hypothetical material characteristics having a threshold level were also modeled. They can be seen in Fig. 6. Obviously, any material with an intensity threshold level would present permittivity modulation only inside a finite volume, when exposed to a microholographic interference pattern. Such recording materials seem to be rare, but do exist [25]. Note, that most experimental work in the literature measure the diffraction efficiency and/or the grating buildup versus exposure time or energy, but not versus power or power density (intensity). In the case of microholographic data storage it would be beneficial to perform investigations in this direction. If the threshold intensity is set to the 1/10 of the maximum intensity occurring in the interference pattern of the microhologram (see Fig. 6), the size of the grating will be large enough and non-addressed layers will show no change in the permittivity, as can be seen in Fig. 7. The gratings have a longitudinal size similar to the two-photon case. This also means that the dynamic range should be divided among bits inside one layer only, similarly to the two-photon case. According to our modeling

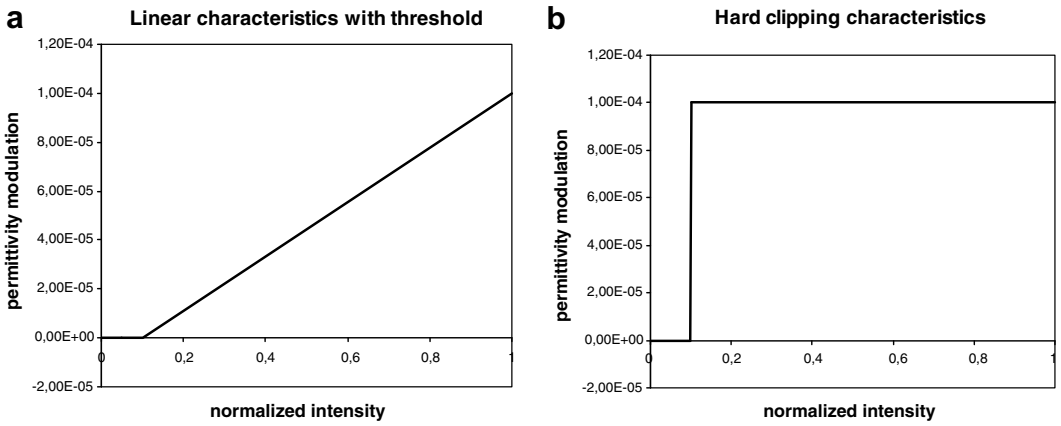

Fig. 6. The permittivity modulation versus intensity characteristics of two hypothetic materials having a threshold level: (a) linear and (b) hard clipping.

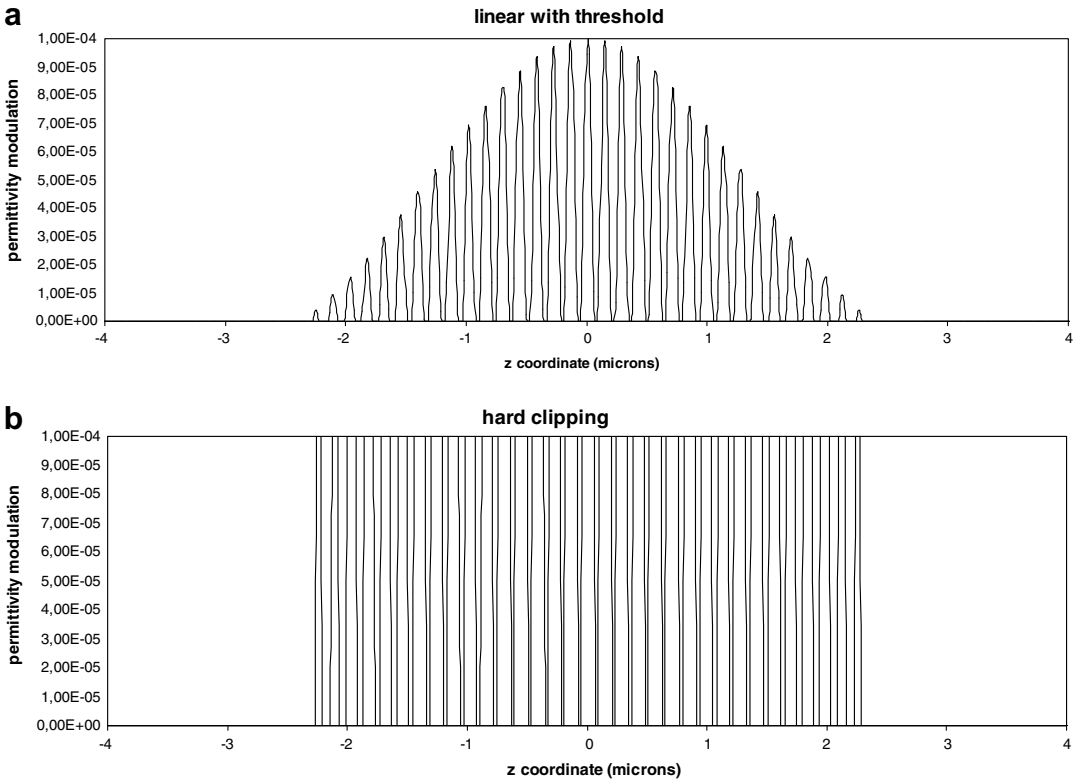

Fig. 7. The longitudinal exposure profile of a microhologram having: (a) thresholded linear and (b) hard clipping characteristics and using diffracting beams. "Sidelobes" are not existing.

results the focus spots in the plane of the confocal filter again have a similar size as in the linear case, and higher order diffracted rings are also present at large propagation angles. To summarize these results, any local intensity dependence seems to keep the good focusability of the reconstructed/diffracted beam, so confocal filtering will stay effective (the divergence angle of the "body" of the beam is also independent from the material characteristics, so aperture losses at the focusing lenses are the same).

In all the non-linear cases above it is a question how does the non-sinusoidal grating profile modify the detectable power behind the confocal filter due to the different diffraction abilities of the gratings. This was also modeled: with all the four types of material a single exposed microhologram had a fixed *maximal* grating strength (in the middle of the hologram) of 10^{-4}. Table 3 shows the detectable power compared to the power of the linear case. As can be seen in the second column, two-photon and thresholded material have lower efficiency, mainly due to the smaller effective volume of the grating. Compared to them the overall maximal grating strength in the case of the hard clipping material is responsible for its high efficiency. The third column shows the situation, when bits are written into 23 layers: the dynamic range has to be divided among the layers in the linear case (due to the previously mentioned globally equal exposure of the layers in this case), but not in the other non-linear cases, so the efficiencies are divided by the number of layers (i.e. 23) in the linear case. The numbers in this column clearly show, that from the viewpoint of the diffraction efficiency either non-linear characteristics are beneficial. The material in Ref. [25] has a characteristic, which starts linearly above the threshold intensity, and for higher intensities it is

Table 3
Normalized diffracted power with different material types

Material characteristics	Detectable power (in a.u.) with one layer...	... and 23 layers
Linear, single-photon	1	0.043
Quadratic, two-photon	0.28	0.28
Linear with threshold	0.54	0.54
Hard clipping	3.98	3.98

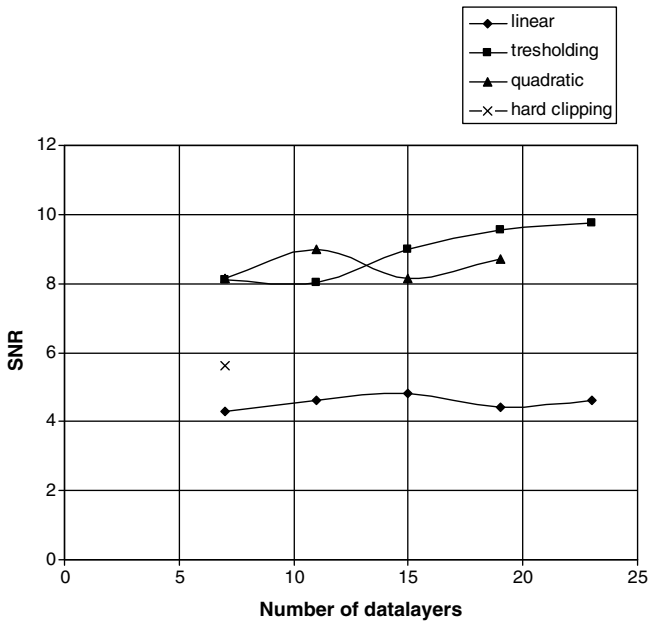

Fig. 8. The raw SNR of the modeled microholographic system versus the number of data layers using four different recording material characteristics.

saturating. Note, that such a real characteristics may be regarded as lying somewhere between the thresholded linear and the hard clipping material.

Finally, Fig. 8 shows the raw SNR of crosstalk related noise of the detected intensities versus the number of data layers for the four different material characteristics discussed. As above in Section 3 the wavelength was 405 nm, the numerical aperture of the system and the beams was 0.6 and the bit and layer spacing was 400 nm by 600 nm by 4 μm. The three non-linear characteristics result in higher SNRs than the conventional linear material or a saturating one with an exposure schedule applied. It is important to note again, that all numbers are based on small statistics, i.e. a few hundred bits, which may leave a significant uncertainty in the results. The results in Fig. 8 are in agreement with Ref. [26], where a slow and reducing change of the SNR is derived with growing layer number for 1D bitwise holographic storage and diffraction efficiencies below 1%.

5. Summary and conclusion

The presented results show that the multilayer thin slice implementation of the perturbative electromagnetic volume integral equation in first-order approximation combined with other scalar diffraction methods is an applicable tool for modeling high density microholographic data storage. The simulation can be adopted to parallel computing easily. The exposure of the 3D set of microholographic gratings and the scattering of the reading beam on the resulting complex grating together with confocal filtering was modeled. The focusing of the beams was ideal due to index matching. Based on the obtained detector signal histograms raw SNR and BER values related to crosstalk noise were estimated. Comparing these at different number of data layers, bit, track and layer spacing, and four kind of local characteristics of the recording material we conclude that the spacing parameters and the material properties have significantly higher influence on crosstalk noise than the number of layers. With 7–23 layers, 400 nm by 600 nm by 4 μm spacing and linear material behavior an SNR about 4.5 was calculated. Quadratic and thresholding material characteristics resulted in less crosstalk noise (i.e. about double SNR), and better use of the dynamic range of the material. Thus by using such materials with non-linear permittivity modulation versus intensity characteristics a further increase of the storage density can be achieved, since neither the SNR nor the diffraction efficiency is affected by the increase of the number of data layers.

Acknowledgements

This research has been supported by the European Union under the project Microholographic Data Disk for Archival Storage (MICROHOLAS) IST 511437, and the Hungarian National Office for Research and Technology under project HEF06-2-BMEHOLO1.

References

[1] H.J. Eichler, P. Kümmel, S. Orlic, A. Wappelt, IEEE J. Sel. Top. Quant. Electr. 4 (1998) 840.
[2] D.A. Waldman, C.J. Butler, D.H. Raguin, Proc. SPIE 5216 (2003) 10.
[3] M. Schnoes, B. Ihas, L. Dhar, D. Michaels, S. Setthachayanon, G.L. Schomberger, W.L. Wilson, Proc. SPIE 4988 (2003) 68.
[4] L. Shiuan Huei, L. June-Hua, C. Po-Lin, S. Yi-Nan, H. Ken Y, J. Nonlinear Opt. Phys. Mater. 15 (2) (2006) 239.
[5] M. Dubois, X. Shi, B.L. Lawrence, E.P. Boden, K.P. Chan, M. Nielsen, L. Hesselink, Characterization of a preliminary narrow-band absorption material for holographic data storage. in: Optical Data Storage Proceedings of SPIE, vol. 5380, September 2004, p. 589.
[6] X. Shi, C. Erben, B.L. Lawrence, E.P. Boden, K.L. Longley, J. Appl. Phys. 102 (1) (2007) 7.
[7] J.T. Sheridan, F.T. O'Neill, J.V. Kelly, J. Opt. Soc. Am. B 21 (2004) 1443.
[8] S. Orlic, E. Dietz, S. Frohmann, C. Mueller, R. Schoen, M. Trefzer, H.J. Eichler, Proc. SPIE 5521 (2004) 161.
[9] S. Orlic, C. Mueller, R. Schoen, M. Trefzer, H.J. Eichler, Proc. SPIE 4459 (2002) 323.
[10] R.R. McLeod, A.J. Daiber, M.E. McDonald, T.L. Robertson, T. Slagle, S.L. Sochava, L. Hesselink, Appl. Opt. 44 (2005) 3197.
[11] Z. Nagy, P. Koppa, E. Dietz, S. Frohmann, S. Orlic, E. Lőrincz, Appl. Opt. 46 (2007) 753.
[12] M. Mansuripur, J. Opt. Soc. Am. A 3 (1986) 2086.
[13] M. Mansuripur, J. Opt. Soc. Am. A 6 (1989) 786.
[14] Peter Kümmel, Analytische und numerische Modellierung von Mikrohologrammen, PhD Thesis, Technische Universität, Berlin, 2004.
[15] J.W. Goodman, Introduction to Fourier Optics, McGraw-Hill, San Francisco, 1996.
[16] J.D. Jackson, in: Classical Electrodynamics, third ed., John Wiley & Sons, New York, 1998, p. 456.
[17] O.J.F. Martin, N.B. Piller, Phys. Rev. E 58 (3) (1998) 3909.
[18] J.J. Goodman, B.T. Draine, P.J. Flatau, Opt. Lett. 16 (15) (1991) 1198.
[19] S.R. Lambourdiere, A. Fukumoto, K. Tanaka, K. Watanabe, Jpn. J. Appl. Phys. 45 (2006) 1246.
[20] B. Gombkötő, P. Koppa, A. Sütő, E. Lőrincz, J. Opt. Soc. Am. A 24 (2007) 2075.
[21] H.J. Coufal, D. Psaltis, G.T. Sincerbox, Holographic Data Storage, Springer-Verlag, 2000.
[22] E. Walker, A. Dvornikov, K. Coblentz, S. Esener, P. Rentzepis, Opt. Express 15 (19) (2007) 12264.
[23] H. Guo, H. Jiang, L. Luo, C. Wu, H. Guo, X. Wang, H. Yang, Q. Gong, F. Wu, T. Wang, M. Shi, Chem. Phys. Lett. 374 (2003) 381.
[24] Y.S. Bai, R.R. Neurgaonkar, R. Kachru, Opt. Lett. 21 (1996) 567.
[25] B.L. Booth, Appl. Opt. 14 (1975) 593.
[26] D.M. Abakoumov, N.A. Ashurbekov, E.H. Gulanian, A.L. Mikaelian, Opt. Mem. Neur. Networks 5 (4) (1996) 295.